UHASSELT
KNOWLEDGE IN ACTION

Maastricht University

Faculty of Medicine and Life Sciences
School for Life Sciences
Master of Biomedical Sciences

Master's thesis

TRPV4 inhibition decreases morphological complexity and the number of filopodia in microglia

Bieke Janssen

Thesis presented in fulfillment of the requirements for the degree of Master of Biomedical Sciences, specialization Molecular Mechanisms in Health and Disease

SUPERVISOR :

Prof. dr. Bert BRONE

MENTOR :

dr. Yeranddy AGUIAR ALPIZAR

2021
2022

Transnational University Limburg is a unique collaboration of two universities in two countries: the University of Hasselt and Maastricht University.

UHASSELT
KNOWLEDGE IN ACTION

www.uhasselt.be
Universiteit Hasselt
Campus Hasselt:
Martelarenlaan 42 | 3500 Hasselt
Campus Diepenbeek:
Agoralaan Gebouw D | 3590 Diepenbeek

UHASSELT
KNOWLEDGE IN ACTION

Maastricht University

Faculty of Medicine and Life Sciences
School for Life Sciences
Master of Biomedical Sciences

Master's thesis

TRPV4 inhibition decreases morphological complexity and the number of filopodia in microglia

Bieke Janssen

Thesis presented in fulfillment of the requirements for the degree of Master of Biomedical Sciences, specialization Molecular Mechanisms in Health and Disease

SUPERVISOR :

Prof. dr. Bert BRONE

MENTOR :

dr. Yeranddy AGUIAR ALPIZAR

TRPV4 inhibition decreases morphological complexity and the number of filopodia in microglia*

Janssen Bieke[1], Mussen Femke[1], Mertens Melanie[2], Bert Brône[2] and Yeranddy A. Alpizar[2]

[1]Biomedical sciences, Faculty of Medicine and Life Sciences, Hasselt University, Campus Diepenbeek, Agoralaan Gebouw D - B-3590 Diepenbeek, Belgium
[2]Neuroscience research group, Biomedical Research Institute, Hasselt University, Campus Diepenbeek, Agoralaan Gebouw C - B-3590 Diepenbeek, Belgium

*Running title: *Mechanosensation via TRPV4 and Piezo1 in microglia*

To whom correspondence should be addressed: Prof. dr. Bert Brône, Tel: +32 (11) 26 92 37; Email: bert.brone@uhasselt.be

Keywords: Microglia, TRPV4, Piezo1, calcium, branch motility, migration, morphology

ABSTRACT

Microglia are essential for maintaining homeostasis and mediating immune responses in the central nervous system (CNS). Their protrusions, also called branches, can scan the entire brain tissue in just a couple of hours. Pathogenic stimuli activate microglia and cause them to migrate towards the stimuli to phagocytize it and release cytokines. This branch motility and migration are dependent on the cell's intracellular calcium concentrations ($[Ca^{2+}]_i$). Besides pathogenic stimuli, microglia can also sense changes in the extracellular matrix (ECM), which include disruptions in cell-cell or cell-ECM signaling and alterations in rigidity, temperature or osmolarity. These mechanical cues are registered with the microglia's mechanosensitive calcium-permeable channels, such as transient receptor potential vanilloid subtype 4 (TRPV4) and Piezo1. However, it is still unclear how exactly these channels influence microglial morphology, migration and branch motility. In this study, we isolated murine eGFP-expressing microglia to study the effect of inhibition and activation of both channels on these processes. Using live-cell imaging techniques, we demonstrated that TRPV4 inhibition decreases morphological complexity and total displacement of microglia. It also reduced branch motility, which was shown in a reduced surveyed area by the filopodia and a decrease in the number and length of filopodia. Further, we determined the functional expression of Piezo1 in wild type and *Trpv4* knockout (KO) microglia.

This study hereby provides a broader molecular framework of how mechanosensitive channels TRPV4 and Piezo1 regulate microglial functions.

INTRODUCTION

As the innate immune cells of the central nervous system (CNS), microglia are essential for neuronal development and homeostasis (1). In the healthy CNS, they help shape neuronal networks by driving neurogenesis and eliminating redundant synapses and apoptotic cells by phagocytosis (2, 3). They display a ramified morphology, with multiple long branches protruding from a small soma. These cells are often referred to as 'resting' microglia, despite being highly motile and constantly monitoring the microenvironment by extending and retracting their branches. The motility needed to survey the brain depends not only on the speed and frequency of these branch extensions and retractions but also on microglial density and the number, length and ramification of the branches (4). In this paper, movement of the branches alone is referred to as branch motility and is used for surveying the healthy adult brain. In contrast, migration refers to the active displacement of the cell soma and generally happens when microglia sense potential threats in the brain (1). When they sense these potentially dangerous signals or normal signaling between microglia and other cells is disturbed, microglia become activated and transform to an amoeboid-like morphology. These

are characterized by a round soma with fewer branches that are shorter and thicker, and migrate towards the stimuli to eliminate it (e.g., to phagocytize a pathogen) (1, 2, 5). However, microglial morphologies are not limited to ramified and amoeboid phenotypes. A large spectrum of morphologies exists between the two, depending on the region of the CNS, activation status of the microglia and sex and age of the organism (2, 6). As the first line of defense, microglia can secrete pro- and anti-inflammatory factors, meaning they can be both neurotoxic and neuroprotective, depending on the microenvironment (2, 3).

This environment, called the extracellular matrix (ECM), is a 3-dimensional network produced by neurons and glial cells and provides support and anchorage to these cells in the CNS. Additionally, its composition and molecular signals drive processes such as cellular growth, activity and survival (7, 8). The ECM consists of three main components. Firstly, the basement membrane, also often referred to as the basal lamina, is located around the cerebral vasculature and is composed of collagen, laminin, nidogen (glycoprotein involved in connecting laminins to collagens), fibronectin and heparan sulphate proteoglycans (perlecans). This basement membrane facilitates cellular interactions between brain capillary endothelial cells, astrocytes and pericytes (8, 9). Secondly, the perineural network surrounds neurons and proximal dendrites and regulates synaptic plasticity. It comprises a hyaluronan backbone, proteoglycans, link proteins and tenascins (7, 10). Lastly, the neural interstitial matrix consists of hyaluronan, tenascins, link proteins, proteoglycans, fibrous proteins (collagen and elastin) and adhesive glycoproteins (laminins and fibronectin) and connects the vasculature and neurons (7, 8). Changes in this ECM can significantly affect cell functions, such as cell migration.

Cell migration and motility are among many processes regulated by $[Ca^{2+}]_i$, such as phagocytosis and cytokine release (11, 12). A rise in $[Ca^{2+}]_i$ influences the structure of the actin cytoskeleton and microtubules, as calcium can directly bind to proteins and induce changes in their conformations, which leads to cell motility and migration (12, 13). However, the exact mechanisms of microglial branch motility and migration are not yet understood. Most of the research in microglia is done on motility and migration in response to injuries and pathologies, in which chemical signaling (e.g., through ATP) plays an important role. The impact and mechanisms of mechanical signaling in microglial movement are still unclear. Several previous studies have investigated how glial cells, such as astrocytes and oligodendrocytes, respond to the stiffness of their environment (14, 15). Microglia were also found to be mechanosensitive and, similar to astrocytes, their morphology becomes more complex on stiffer substrates (16). When microglia are cultured on a stiffness gradient substrate, they preferentially migrate towards the more rigid regions. This process is called durotaxis (16). To sense the mechanical properties of the environment – and subsequently act accordingly – microglia are equipped with various mechanosensitive receptors and channels. These convert mechanical stimuli, such as cell stretching or osmotic pressure, into an intracellular signal (17). One way cell-ECM interactions are mediated is through integrins. Integrin binding to the ECM triggers an outside-in signaling cascade that regulates the cytoskeleton (18). However, Kim *et al*. have shown that the deformation of a cell membrane, either through mechanical force or curvature, can induce integrin activation (19). Another receptor type that influences the cytoskeleton, and thus the shape and movement of the cell, is the G protein-coupled receptor family (GPCRs). These receptors affect cytoskeleton remodeling by activating small GTP-binding proteins of the Rho GTPases family and modulating cAMP levels (18). GPCRs can bind to a variety of ligands, including ions, photons, hormones (e.g., angiotensin), proteins (e.g., chemokines), neurotransmitters (e.g., serotonin, dopamine) and some metabolites (e.g., ATP, ADP, fatty acids and bile acids) (20). But more specifically, adhesion GPCRs, one of the five main GPCR families, have been shown to be able to strongly interact with the ECM (by binding to collagens and laminins) and thus can be activated by mechanical cues (21). Besides receptors, ion channels are also involved in mechanosensation. One such family of ion channels is the transient receptor potential (TRP) family. These consist of non-selective cation channels that can be activated not only by mechanical but also thermal and chemical stimuli. Microglia express some receptors from this family, such as TRPV (vanilloid), TRPM (melastatin) and TRPC (canonical) (22). Of these

channels, TRPV4 is being studied intensively for its function in microglial activity. It is a non-selective channel permeable to calcium and magnesium ions, among others, and is expressed in a wide variety of non-neuronal cells (including smooth muscle cells, epithelial cells and macrophages), as well as in the CNS (neurons, astrocytes and microglia) (22-24). TRPV4 can be activated by various endogenous stimuli, such as cell swelling, stretch, mechanical stress and a change in osmolarity, temperature or pH (22, 25, 26). Nishimoto *et al*. have previously determined that in physiological conditions, microglial movement is affected by a change in temperature *in vitro* and *in vivo*. In TRPV4 knockout microglia, this temperature-dependency was lost in both physiological and pathological conditions *in vivo* (27). Another study has found that acute inhibition of TRPV4 decreases the branch motility of microglia *in vitro*. In a TRPV4 knockout model, on the other hand, motility was not affected (Beeken *et al*., second revision). Therefore, another mechanism is believed to be present for mechanical sensing and taking over the function of TRPV4 in the knockout model. Piezo1 is a calcium-permeable ion channel that reacts to mechanical stimuli such as tension created by interactions with the ECM, membrane stretching and osmotic pressure (17). This channel was identified in 2010 by Ardem Patapoutian, for which he was awarded the 2021 Nobel Prize in Physiology or Medicine (28, 29). Research on this recently identified channel is still limited. A few studies have investigated the role of Piezo1 in bone formation and angiogenesis and Piezo1 has also been found to be involved in the mechanoregulation of red blood cell volume and differentiation of neural stem cells (30-33). However, its function in microglia remains to be elucidated.

This study aims to investigate the role of both TRPV4 and Piezo1 in microglial branch motility and migration and provide a molecular framework to better understand the fundamental mechanisms for microglial movement.

EXPERIMENTAL PROCEDURES

Animals – In this study, eGFP-expressing wild type (WT) and *Trpv4*$^{-/-}$ C57BL/6 mice were used. All animals were obtained by in-house breeding and genotyped with PCR (Suppl. info). They were housed in the Biomedical Research Institute (BIOMED) animal facility on a 12 h light/dark cycle with access to water and food *ad libitum*. All animal experiments were conducted in accordance with the European Community guiding principles on the care and use of animals and with the approval of The Ethical Committee of Hasselt University.

Cell lines – BV_2 cells were cultured in DMEM (Sigma-Aldrich) supplemented with 10% FCS and 1% Penicillin/Streptomycin (P/S, Lonza, Switzerland) and kept at 37 °C and 5% CO_2.

Primary microglia isolation – Primary microglia were isolated from 21-day-old pups (P21), as described by Bohlen *et al*. (34). Pups were decapitated, after which their brain was removed and transferred to cold DMEM with 1% P/S. Under a flow, the brains were triturated, and papain (17 U/mg, Sigma-Aldrich) and DNase I (Roche, Switzerland) were added to further degrade them. After 15 min incubation at 37 °C, the solution was gently mixed and incubated again for 15 min at 37 °C. Next, the cells were passed through a 70 µm cell strainer. The cell suspension was then centrifuged for 5 min at 500G at room temperature (RT). After aspirating the supernatant, the cell pellet was resuspended in 5 ml of 30% stock isotonic percoll (SIP, Percoll, GE Healthcare, USA). The solution was transferred to a new 15 ml tube, and using a pipet boy with setting G (gravity), 3 ml of 70% SIP was pipetted at the bottom of the 15 ml tube, resulting in a 70% - 30% gradient. After adding 2-3 ml PBS 1x on top, the gradient was centrifuged for 25 min at 650G at RT, with brake at 0 and acceleration at 4. Next, the myelin layer and part of the media were aspirated before collecting the mononuclear cells at the 70-30% interface and mixing them with 1x PBS to aid removal of the density gradient medium. After centrifuging for 5 min at 500G at 4 °C, microglia were isolated from the cell suspension using magnetic bead separation (Miltenyi Biotec, Germany), targeting CD11b+ cells (macrophage and microglia marker). The microglia were seeded on well plates precoated with poly-D-lysine (PDL, Gibco) and collagen-IV (Sigma-Aldrich). They were kept on 10:10:1 medium (10% horse serum, 10% fetal calf serum, 1% P/S in high-glucose DMEM) for one week, before the medium was changed to serum-free TIC medium (DMEM/F12 (Sigma-Aldrich) supplemented with 1% P/S, Na^+ Selenite (0.1 µg/ml), insulin (5 µg/ml), apo-transferrin (100

µg/ml), heparan-sulfate (1 µg/ml), acetyl-cysteine (5 µg/ml), human TGFβ2 (2 µg/ml), cholesterol (1.5 µg/ml), murine IL-34 (0.1 µg/ml) and L-glutamine (3 µg/ml)) for one week (35). The murine microglia were always kept at 37 °C and 8% CO_2.

Microglial morphology and movement – WT and *Trpv4*$^{-/-}$ murine microglia cultured in a 24-well plate were incubated with TRPV4 antagonists RN9893 (RN, Tocris Bioscience, UK), HC067047 (HC, Tocris Bioscience, UK) and GSK2193874 (GSK21, Tocris Bioscience, UK) (1 µM or 10 µM) and imaged for 24 h using the Incucyte S3. WT microglia cultured in a 24-well plate were incubated with TRPV4 agonist GSK1016790A (0.5 µM or 1 µM) (GSK101, Tocris Bioscience, UK) and Piezo1 agonist Yoda1 (Tocris Bioscience, UK) (0.1 µM or 0.2 µM). DMSO (0.02%) was used as a control treatment. Images were captured every 10 min for 6 consecutive hours. After 24 h of incubation, the last image was captured. Images were analyzed with Fiji. Cell contours were manually defined for morphology, and shape parameters were quantified at various time points. Microglial movement was measured by manually tracking the cells and quantifying the migration distance.

Live-cell filopodia imaging – WT isolated murine microglia were seeded on a 24-well plate with glass bottoms (Ibidi, Germany) and cultured as described before. Before imaging, the medium was taken out of the well and replaced with Krebs solution (pH 7.4, 150 mM NaCl, 6 mM KCl, 1.5 mM $CaCl_2$, 1 mM $MgCl_2$, 10 mM HEPES and 10 mM glucose monohydrate). After 5 min of incubation, timelapse live-cell images were made every 10 sec for 3 min (control), using the Zeiss LSM880 confocal microscope with a 63x oil immersion objective. Next, 10 µM RN or HC was added to the well. Images were taken again after a 5 min incubation. Afterward, all images were acquired using the Airyscan detector coupled to the LSM880 microscope. All images were analyzed in Fiji by manually defining the scanned area of a cell and the filopodia.

Live-cell Ca^{2+} imaging – WT and *Trpv4*$^{-/-}$ murine microglia were isolated and cultured in glass chambers. BV_2 cells were cultured in hydroxy-PAAm hydrogels made in glass chambers. Both cell types were incubated with Fluo-4 (fluorescent Ca^{2+} indicator, 2 µM, ex/em 494/506 nm, Invitrogen, USA) for 35 min (isolated microglia) or 20 min (BV_2 cells) at 37° C. For these experiments, murine microglia that did not express eGFP were used due to overlapping emission/excitation spectra with Fluo-4. During imaging, microglia were continuously perfused with Krebs solution. Timelapse live-cell Ca^{2+} imaging was performed with Zeiss Elyra PS.1 widefield fluorescence microscope with a 488 nm excitation laser and a laser power of 1%. Images were captured at one frame per second using a PCO Edge 4.2 sCMOS camera connected with an Ander iXon+ 897 EMCCD camera at a magnification of 10x. The first 120 sec represent the microglia in Krebs solution (baseline). Between 120 and 240 sec, Piezo1 agonist Yoda1 was added in 10 µM, 30 µM or 50 µM, diluted in Krebs. Next, the cells were perfused in Krebs solution again for 4 min, followed by adenosine triphosphate (ATP, 10 µM) for 1 min as a control (**Figure 3B**). Acquired images were processed with Fiji (ImageJ v2.0, Open source software). For each time point, the mean pixel intensity in the soma was calculated. The amplitude of Yoda1 activation was calculated and normalized by the average pixel intensity of the baseline (90-120 sec). Microglia were counted as reactive cells when their maximum pixel intensity during Yoda1 activation was above the baseline (90-120 sec) plus five times the standard deviation.

Hydroxy-polyacrylamide (PAAm) hydrogels – Hydroxy-PAAm hydrogels were made following a protocol adapted from Grevesse *et al*. (36). First, circular glass coverslips (18 mm diameter) were activated by treating them with 0.1 M NaOH. After washing the coverslips twice with sterile ddH_2O for 20 min, they were dried with high-purity nitrogen gas. Next, the coverslips were treated with a thin layer of 3-(trimethoxysilyl)propyl acrylate (92%) (Sigma-Aldrich). They were then extensively washed with and immersed in sterile ddH_2O. After gently rocking them for 10 min, the coverslips were removed from ddH_2O with sterile tweezers and placed in a new Petri dish with the activated side up.

To prepare the hydroxy PAAm hydrogels, 65 µl of N-hydroxyethyl acrylamide (HEA, Sigma-Aldrich) was mixed with 1 ml of 50 mM HEPES buffer (HEPES powder, VWR Chemicals). Next,

400 µl of 40% w/w in HEPES acrylamide solution (acrylamide powder, Sigma-Aldrich) and the required volume of 2% w/w in HEPES bis-acrylamide solution (N,N′-Methylenebis(acrylamide), Sigma-Aldrich) were added to the HEA solution to achieve the wanted hydrogel stiffness (**Table 1**). HEPES (50 mM) was added to reach a total volume of 5 ml. Afterward, the solution was degassed in a vacuum chamber for 20 min before being filtered with a 0.2 µm pore size filter to sterilize it. Circular glass coverslips (12 mm diameter) were activated in a UV/ozone cleaner for 7 min. 2.5 µl of N,N,N′,N′-Tetramethylethylenediamine (TEMED, Sigma-Aldrich) and 25 µl of freshly prepared 10% ammonium persulfate (APS, Sigma-Aldrich) were added to the sterilized hydroxy-PAAm solution. A 13 µl drop of the hydroxy-PAAm solution was then placed on the 18 mm glass coverslip. Next, a 12 mm glass coverslip was immediately placed on top of the droplet, with the activated side down. After polymerization, the coverslips were fully immersed in sterile ddH_2O. The 12 mm glass coverslip was detached by inserting the edge of a razor blade between the top coverslip and the hydrogel. The 18 mm glass coverslips with the hydroxy-PAAm hydrogels were placed in a well-plate and rinsed with PBS before being coated and incubated with a PDL solution only (for BV_2 cells) or a PDL and collagen solution (for isolated microglia).

Statistics – Statistical analyses were performed using GraphPad Prism 8 (GraphPad Software, USA). The Shapiro-Wilk test was used to check the normality of data. When comparing two groups, the unpaired, two-tailed Mann-Whitney test was used. Multiple groups were compared using a Kruskal-Wallis test with Dunn's correction for multiple comparisons. Paired data were analyzed using a Wilcoxon matched-pairs Signed-rank test. Categorical data classified in two different ways were analyzed using Fisher's exact t-test. Differences with p values <0.05 are considered significant.

RESULTS

Microglial morphology and total displacement following acute TRPV4 inhibition – TRPV4 has been shown to play a role in microglial morphology and branch motility upon osmotic stress and thermosensation (25, 27). Beeken *et al*. (second revision) have previously determined the effect of TRPV4 antagonist GSK21 on microglial morphology and migration. They showed that TRPV4 inhibition with GSK21 significantly reduced morphological complexity of WT microglia. To further validate these results and test if this is a general effect of TRPV4 inhibition, we studied the effect of two other TRPV4 inhibitors, RN9893 and HC067047, on microglial morphology and migration using live-cell imaging (**Figure 1**). Murine WT eGFP-expressing microglia were isolated via magnetic bead separation targeting CD11b (microglia marker), according to Bohlen *et al*. and cultured as described above (34).

Following administration of 1 µM or 10 µM of TRPV4 antagonists RN and HC, images were captured every 10 min for 6 consecutive hours and the last image was made after 24 h of incubation. Morphological complexity of WT microglia was visually decreased after 24 h incubation with 10 µM HC, while RN seemed less potent (**Figure 1A**). Circularity and area measurements were quantified after 0.5 h, 6 h and 24 h of administration of DMSO (0.02%) and 1 µM or 10 µM of TRPV4 antagonists RN or HC (**Figure 1B, C**). A low circularity represents complex ramified microglial morphology. Microglia exposed to 1 µM and 10 µM HC showed a significantly higher circularity after 0.5 h and 6 h ($p<0.0001$) compared to a control condition (0.02% DMSO), while there were no significant differences after 1 µM or 10 µM of RN incubation (**Figure 1B**).

Table 1: Preparation of hydroxy-PAAm hydrogels with various rigidities. Compositions of solutions to achieve hydroxy-PAAm hydrogels with final stiffness of 1.4, 8.7 and 25 kPa (modified from (36)).

Final AAm/bisAAm ratio	AAm 40% (µl)	Amount of HEA to dissolve in 1 ml HEPES (µl)	bisAAm 2% (µl)	HEPES (µl)	Young's modulus (10^3 Pa)
0.2/50	400	65	50	3.485	~ 1.4
1/50	400	65	250	3.285	~ 8.7
3/50	400	65	750	2.785	~ 25
Aam: acrylamide, bisAAM: bis-acrylamide, HEA: N-hydroxyethyl acrylamide, Pa: Pascal					

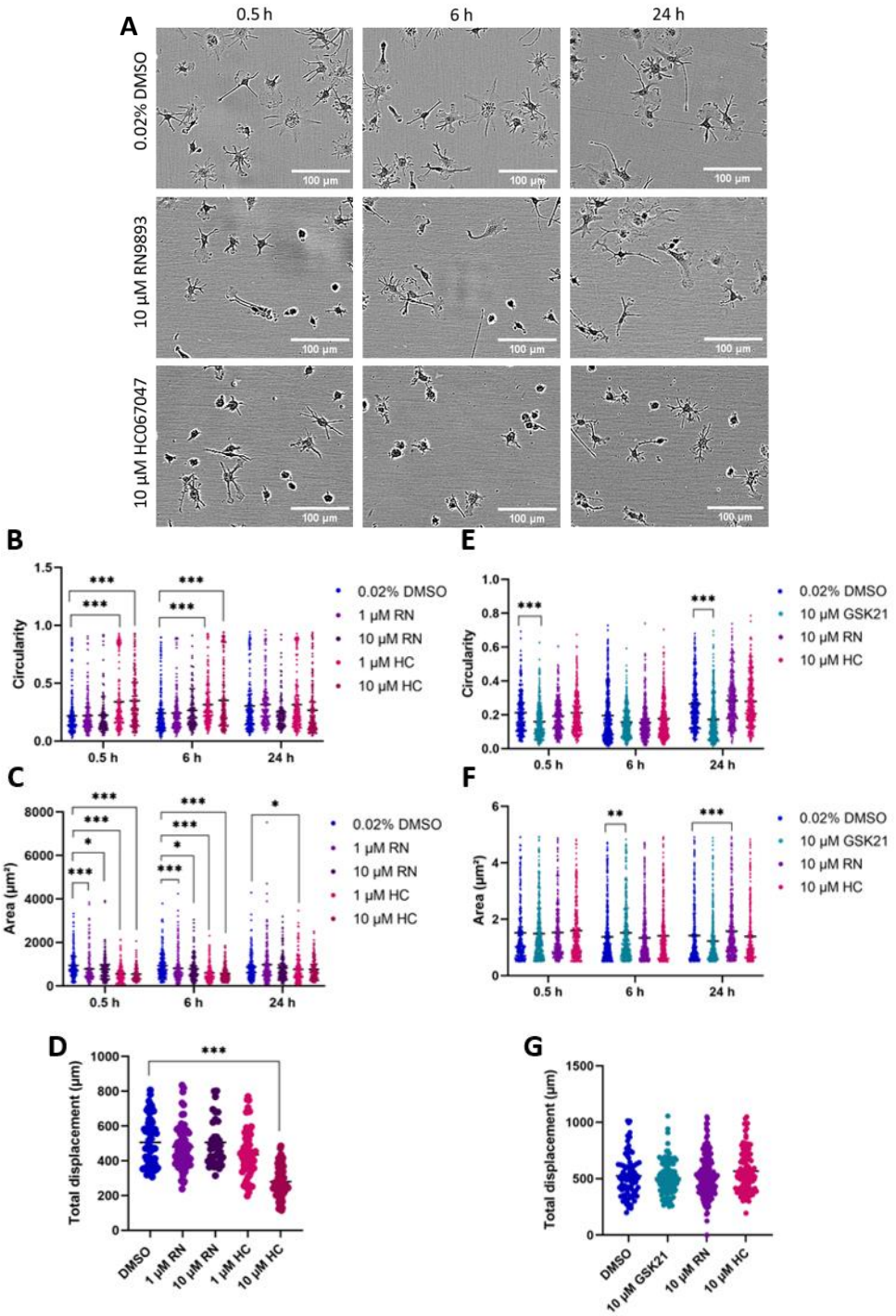

Figure 1: Morphological characterization and total displacement of murine WT and *Trpv4*$^{-/-}$ (KO) microglia after TRPV4 inhibition. (**A**) Representative live-cell images of murine WT microglia incubated with 0.02% DMSO (control) or 10 µM TRPV4 antagonist (RN or HC) at various timepoints. Images were taken every 10 min for 6 consecutive hours and a final image after 24 h. (**B-C**) Circularity and area measurements of WT microglia incubated with DMSO, 1 µM or 10 µM of RN or HC for 0.5 h, 6 h and 24 h. After manually defining cell contours, circularity and area measurements were quantified using Fiji (n > 202 cells/condition). (**D**) Total displacement of WT microglia incubated with DMSO, 1 µM or 10 µM of RN or HC for 0.5 h, 6 h and 24 h. Cells were manually tracked over 6 hours and the total displacement was quantified using Fiji (n > 38 cells/condition). (**E-F**) Circularity and area measurements of KO microglia incubated with DMSO or 10 µM of GSK21, RN or HC for 0.5 h, 6 h and 24 h (n > 293 cells/condition). (**G**) Total displacement of KO microglia incubated with DMSO or 10 µM of GSK21, RN or

HC for 0.5 h, 6 h and 24 h (n > 83 cells/condition). Data is represented as mean ± SEM and analyzed with a Kruskal-Wallis test with Dunn's correction for multiple comparisons. *p<0.05, **p<0.01, ***p<0.001.

Both 1 µM and 10 µM of RN and HC significantly reduced cell area after 0.5 h (p<0.0001 for 1 µM RN, p=0.0032 for 10 µM RN and p<0.0001 for 1 µM and 10 µM HC) and 6 h (p=0.0006 for 1 µM RN, p=0.0147 for 10 µM RN and p<0.0001 for 1 µM and 10 µM HC) incubation. After 24 h, only the microglia incubated with 1 µM HC still had a reduced cell area (p=0.0175) (**Figure 1C**). In general, TRPV4 inhibition decreases morphological complexity of WT microglia. Inhibition with RN did not affect total displacement of microglia over 6 h. In contrast, HC administration of 10 µM showed a significant decrease in total displacement (p<0.0001) (**Figure 1D**). Next, *Trpv4*$^{-/-}$ microglia were inhibited with 10 µM of GSK21, RN or HC to assess possible side effects of TRPV4 inhibition (**Figure 1E-G**). GSK21 significantly decreased circularity at 0.5 h and 24 h (p<0.0001) and area at 6 h (p=0.0015). RN significantly reduced cell area only after 24 h (p=0.0004) (**Figure 1E, F**). None of the TRPV4 inhibitors significantly reduced total displacement of the *Trpv4*$^{-/-}$ microglia (**Figure 1G**). TRPV4 inhibition thus does not lead to any side effects.

TRPV4 inhibition leads to reduced number and length of filopodia and branch motility – In a similar setting, after murine WT microglia isolation and culture, we performed timelapse live-cell imaging of the cell's filopodia before and after TRPV4 inhibition with 10 µM RN or HC to assess microglial branch motility (**Figure 2A**). Both RN and HC significantly reduced the surveyed area of the cell (p=0.016 and p=0.0016, respectively), as well as the number of filopodia (p=0.0112 and p=0.008, respectively) (**Figure 2B-E**). Filopodia length was also significantly reduced after inhibition with both antagonists (p<0.0001) (**Figure 2F**). Both inhibitors thus decrease microglial branch motility by reducing the number and length of filopodia.

Functional expression of Piezo1 in WT and Trpv4$^{-/-}$ *murine microglia* – The previous experiments have shown TRPV4 to be important in microglial morphology, movement and branch motility. However, Beeken *et al*. (second revision) found that acute TRPV4 inhibition did not affect branch motility in a *Trpv4*$^{-/-}$ mouse model. So, the question remains if microglia express other mechanosensation channels involved in processes such as morphology and migration. And if so, do these channels take over the regulation of these processes in a *Trpv4*$^{-/-}$ model? We first determined the gene expression profile of mechanosensitive channels *Piezo1*, *Piezo2*, *Trpm7* and *Trpm2* in WT

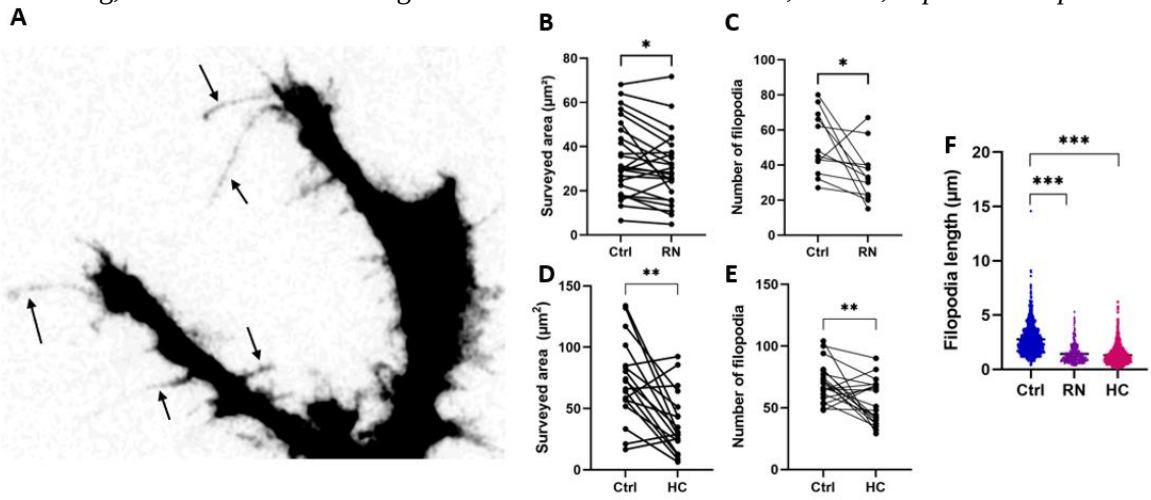

Figure 2: TRPV4 inhibition decreases branch motility in murine WT microglia. (A) Representative image of a WT microglia with filopodia (arrows). **(B-C)** Surveyed area (n=25) and the number of filopodia (n=12) of WT microglia before (ctrl) and after TRPV4 inhibition with 10 µM RN. (**D-E**) Surveyed area (n=18) and the number of filopodia (n=20) of WT microglia before (ctrl) and after TRPV4 inhibition with 10 µM HC. (**F**) Filopodia length of WT microglia before (ctrl) and after inhibition with 10 µM of RN or HC (n= min. 416, max 1408). Data is represented as (**F**) mean ± SEM and analyzed with (**B-E**) Wilcoxon matched-pairs signed-rank test and (**F**) Kruskal-Wallis with Dunn's correction for multiple comparisons. Ctrl: control. *p<0.05, **p<0.01, ***p<0.001.

and *Trpv4*$^{-/-}$ murine microglia via quantitative real-time qPCR (Suppl. info) (**Figure 3A**). However, none of these channels showed a significant increase in gene expression in *Trpv4*$^{-/-}$ microglia. Next, the functional expression of *Piezo1* was further investigated using live-cell Ca^{2+} imaging (**Figure 3B**). Ca^{2+} response was measured during acute Piezo1 stimulation (120-240 sec) with Yoda1 (**Figure 3C-D**). The percentage of reactive WT and *Trpv4*$^{-/-}$ microglia was calculated by comparing the maximum value during acute Piezo1 stimulation (120-240 sec) to the baseline (90-120 sec) plus five times the standard deviation (**Figure 3E, G**). In WT microglia, significantly more cells reacted to 30 µM of Yoda1 (19.14%), compared to 10 µM (2.73%) or 50 µM (7.69%) (p=0.0012 and p=0.0002, respectively) (**Figure 3E**). In contrast, the amplitude of the Ca^{2+} response was not significantly different after administration of 10 µM, 30 µM or 50 µM of Yoda1 (**Figure 3F**). In the *Trpv4*$^{-/-}$ microglia, the highest percentage of cells reacted to 50 µM of Yoda1 (27.56%). Only 14.23% and 10.97% of cells responded to 10 µM and 50 µM of Yoda1, respectively (**Figure 3G**). As for the response itself, we measured a significantly higher increase in $[Ca^{2+}]_i$ in the *Trpv4*$^{-/-}$ cells after administration of 50 µM Yoda1 compared to 10 µM and 30 µM Yoda1(p=0.0003) (**Figure 3H**). When comparing the Ca^{2+} response between the two genotypes (WT and *Trpv4*$^{-/-}$), data show a significant difference after Piezo1 stimulation with 30 µM (p=0.0257) and 50 µM (p=0.0163) of Yoda1 (**Figure 3I**). In general, it can be stated that Piezo1 is functionally expressed both in the presence and absence of TRPV4.

TRPV4 and Piezo1 activation in WT murine microglia lead to decreased morphological complexity 0.5 h after activation – Next, we investigated the behavior of microglia after TRPV4 and Piezo1 activation instead of inhibition (**Figure 4**). Nishimoto *et al*. observed increased $[Ca^{2+}]_i$ and enhanced migration of microglia after TRPV4 activation with GSK101. They also evaluated total process length and number of branches per cell following TRPV4 stimulation (27). Therefore, we examined the effect of TRPV4 and Piezo1 activation on the morphology of WT microglia. Visually, there do not seem to be any differences after administration of 1 µM of GSK101 or 0.2 µM of Yoda1 (**Figure 4A**). Circularity and area measurements 0.5 h, 6 h and 24 h after administration of both agonists were again measured by manually defining cell contours and quantifying them using Fiji. Following 0.5 µM or 1 µM of GSK101 administration, microglia showed a significant increase in circularity after 0.5 h (p=0.0072 and p=0.0127, respectively) compared to the control treatment. In contrast, after 24 h of 0.5 µM GSK101 incubation, the circularity was significantly lower (p=0.0211). This was not seen after 24 h of 1 µM GSK101 incubation (**Figure 4B**). Both 0.5 µM and 1 µM of GSK101 significantly lowered cell area after 5 h (p<0.0001 and p=0.001, respectively), 6 h (p<0.0001 and p=0.0003, respectively) and 24 h (p<0.0001 for both conditions) (**Figure 4B**). Piezo1 stimulation with 0.2 µM of Yoda1 resulted in a significant increase in cell circularity after 0.5 h (p<0.0001). Just like the GSK101 condition, after 24 h incubation with 0.1 µM and 0.2 µM Yoda1, microglia showed a significant reduction in circularity (p=0.0022 and p<0.0001, respectively) compared to the control treatment (**Figure 4C**). Piezo1 activation with 0.1 µM and 0.2 µM both significantly decreased cell area after 0.5 h (p=0.0002 and p<0.0001, respectively), 6 h (p=0.0009 and p<0.0001, respectively) and 24 h (p=0.0001 and p<0.0001, respectively) (**Figure 4C**).

Therefore, we can state that both activation of TRPV4 and Piezo1 lead to a decreased morphological complexity 0.5 h after incubation with the agonist. This effect is lost already after 6 h incubation, with even an increase again in morphological complexity.

Piezo1 expression in BV_2 cells cultured in hydroxy-PAAm hydrogels – Lastly, we wanted to examine the effect of the stiffness of the ECM on microglial morphology and migration. As Bollman *et al*. have demonstrated that microglia display durotaxis (preferential migration towards stiffer regions), we wanted to study if and how Piezo1 is involved in this migration (16). For this, we used hydroxy-polyacrylamide (PAAm) hydrogels, following a protocol of Grevesse *et al*., as these

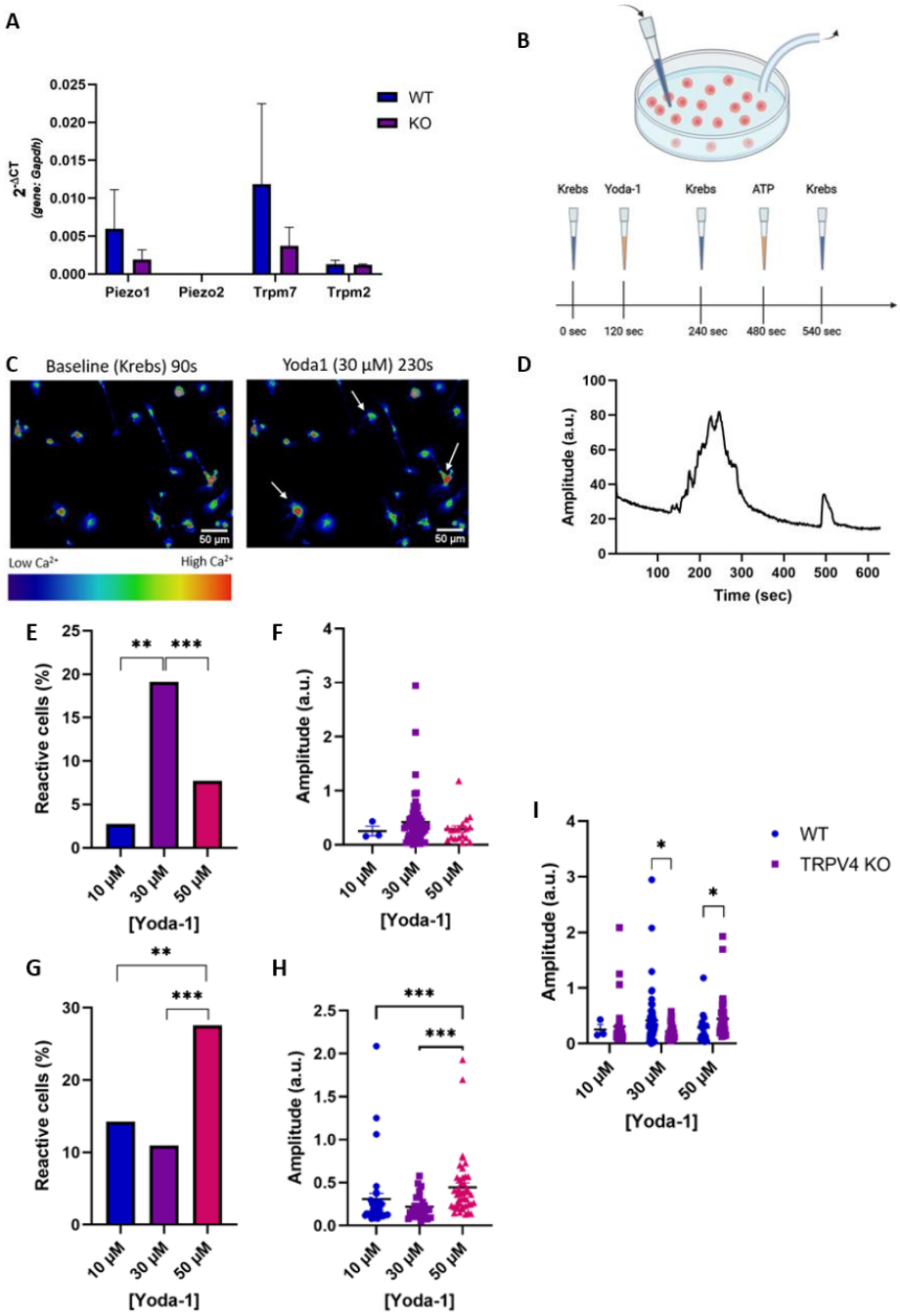

Figure 3: Gene and functional expression of Piezo1 in murine WT and *Trpv4*$^{-/-}$ (KO) microglia. (A) Gene expression profile of *Piezo1*, *Piezo2*, *Trpm7* and *Trpm2* in WT (n= 3) and *Trpv4*$^{-/-}$ (n= 3) murine microglia presented in $2^{-\Delta ct}$ with *Gapdh* as a reference gene. (**B**) Overview of the setup and treatments with the time schedule for the Ca^{2} imaging experiments. (**C**) Representative images of Fluo-4 labeled WT microglia before (90 sec) and during Piezo1 stimulation (230 sec, examples of reactive cells shown by white arrows) with 30 µM of Yoda1. (**D**) Representative Ca^{2+}-influx trace of WT microglia throughout live-cell Ca^{2+} imaging of acute Piezo1 stimulation with 30 µM Yoda1, showing 1 peak during Yoda1 stimulation (120-240 sec) and 1 peak during ATP stimulation (480-540 sec). (**E, G**) Percentage of (**E**) WT and (**G**) KO cells reactive to Yoda1 stimulation with 10 µM (WT: 2.73%, KO: 14.23%), 30 µM (WT: 19.14%, KO: 10.97%) or 50 µM (WT: 7.69%, KO: 27.56%). (**F, H**) Ca^{2+} response of reactive (**F**) WT and (**H**) KO microglia represented as the amplitude during administration of 10 µM, 30 µM or 50 µM of Yoda1 (n = min 3, max 58). (**I**) Ca^{2+} response of WT compared to KO microglia during administration of 10 µM, 30 µM or 50 µM of Yoda1. Data are represented as mean ± SEM and analyzed using (**A, I**) Mann-Whitney test, (**E, G**) Fisher's exact test and (**F, H**) Kruskal-Wallis with Dunn's correction for multiple comparisons. *p<0.05, **p<0.01, ***p<0.001.

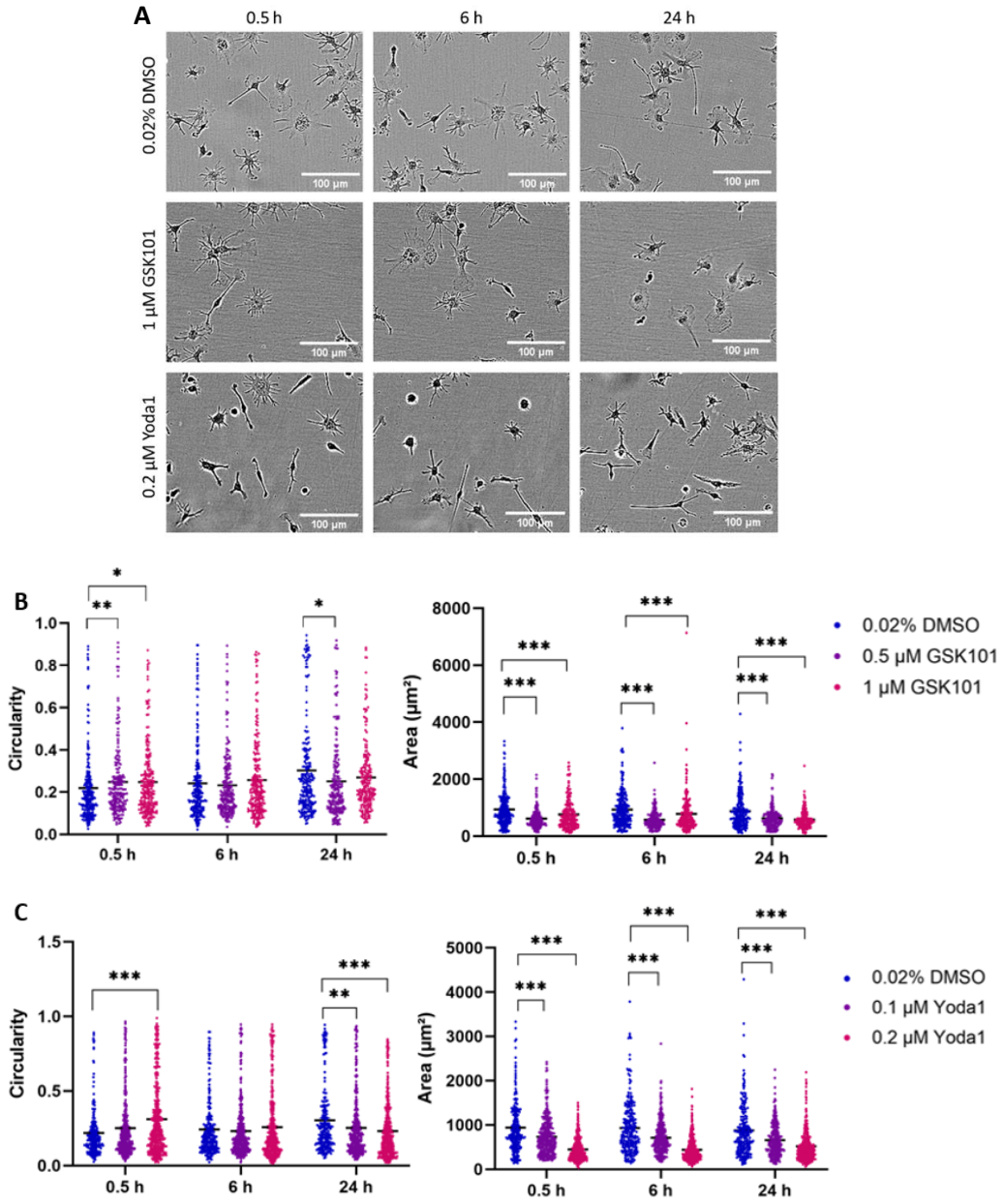

Figure 4: Morphological characterization of murine WT microglia following TRPV4 and Piezo1 activation. (**A**) Representative live-cell images of murine WT microglia incubated with 0.02% DMSO (control), 1 µM GSK101 or 0.2 µM Yoda1 at various timepoints. Images were taken every 10 min for 6 consecutive hours and a final image was captured after 24 h. (**B**) Circularity and area measurements of WT microglia incubated with DMSO, 0.5 µM or 1 µM of GSK101 for 0.5 h, 6 h and 24 h. After manually defining cell contours, circularity and area measurements were quantified using Fiji (n >204 cells/condition). (**C**) Circularity and area measurements of WT microglia incubated with DMSO, 0.1 µM or 0.2 µM of Yoda1 for 0.5 h, 6 h and 24 h (n > 216 cells/condition). Data are represented as mean ± SEM and analyzed using Kruskal-Wallis with Dunn's correction for multiple comparisons. *p<0.05, **p<0.01, ***p<0.001.

allow us to independently modulate substrate stiffness (**Figure 5A, B**) (36). We first optimized the protocol to produce hydroxy-PAAm hydrogels of 1.4 kPa, 8.7 kPa and 25 kPa. Before using isolated murine microglia, we seeded BV_2 cells (microglial cell line) on the hydrogels to evaluate their cell attachment and behavior in the gels. After 5 days in culture, cells were visually checked, and they seemed to attach well to the hydrogels. There was also a visual difference in morphology: BV_2 cells cultured on the softest substrate (1.4 kPa) displayed a rounder phenotype, while in the hardest

substrate (25 kPa), cells were generally more stretched out (**Figure 5D-F**). After seeing BV_2 cells survive in and attach to the hydrogels, we proceeded to evaluate the functional expression of Piezo1 in BV_2 cells cultured in these conditions. Live-cell Ca^{2+} imaging was performed, following the same setup and time schedule as used in isolated microglia (**Figure 3B**). $[Ca^{2+}]_i$ was measured during Piezo1 stimulation with 10 µM of Yoda1 (240-480 sec) (**Figure 5G, H**). In the substrates of 1.4 kPa, cells showed the least amount of reactive cells (37.9%) compared to substrates of 8.7 kPa (61.11%) and 25 kPa (78.26%) ($p=0.0019$ and $p<0.0001$, respectively) (**Figure 5I**). $[Ca^{2+}]_i$ increased the highest in BV_2 cells cultured in 25 kPa hydrogels in comparison to the other two conditions ($p<0.0001$), while the responses in 1.4 kPa and 8.7 kPa hydrogels were relatively equal to each other (**Figure 5J**).

Thus, there seems to be either activation of more Piezo1 channels or a more efficient activation of the Piezo1 channels in BV_2 cells cultured on stiffer substrates.

Next, we tried to optimize the protocol for using isolated murine WT microglia in these hydroxy-PAAm hydrogels. However, microglia did not attach very well to the hydrogels. In the softer substrates, they even seemed to migrate out of the hydrogel towards the glass coverslip. Therefore, we produced custom-made Teflon rings to place over the hydrogel on the coverslips before seeding the cells (**Figure 5C**). These would prevent the cells from migrating towards the glass coverslip and keep them centered in the hydrogels instead. After placing the rings over the hydrogels, murine microglia were seeded in the center of it and cultured as described before. After 1-2 days in culture, the Teflon rings were removed. Unfortunately, the difficulties regarding the attachment of microglia to the hydrogels remained and we were not able to fully optimize this protocol within the duration of this study.

DISCUSSION

Microglia are the primary immune cells of the CNS and are essential during development and adulthood to maintain homeostasis (1). In the healthy state, they are ramified with multiple branches extending from the soma, with which they survey the brain tissue (1, 2). Microglial dysfunction is involved in several neurological pathologies (37). So, it is crucial to understand the underlying mechanisms of microglial functions. Ca^{2+}-influx is essential to regulate microglial motility and migration since it allows cytoskeleton remodeling by stimulating actin polymerization (4, 38). Recent research has found that TRPV4 plays a role in thermo- and mechanosensation of microglia and that channel manipulation affects microglial morphology, motility and migration (4, 25, 27). Beeken *et al*. (second revision) showed that acute TRPV4 inhibition using GSK21 decreases morphological complexity (meaning fewer branches and ramifications) and reduces microglial migration distance. In this study, we further determine the influence of TRPV4 on microglial morphology and migration. Secondly, we study Piezo1, a different mechanosensitive calcium-permeable channel, and its role in microglial functions. Lastly, as microglia have been found to be mechanosensitive, we wanted to investigate how morphology and migration are affected by the mechanical properties of the ECM, such as its stiffness (16).

To establish the effect of TRPV4 inhibition on microglial morphology and movement, we first isolated murine primary microglia. Before using them in experiments, they were cultured in specific culture conditions (35). We wanted to test if the effect Beeken *et al*. found is a general effect of TRPV4 inhibition or exclusively by inhibition with GSK21 by incubating isolated microglia with TRPV4 inhibitors RN9893 and HC067047 for 24 h. We determined that HC decreased morphological complexity (by increasing cell circularity) until 6 h after incubation. RN seemed to be less potent in inhibiting TRPV4. At first, we believed this to be due to differences in the IC_{50} values. In mice, RN has an IC_{50} value of 320 nM, while HC has a value of only 17 nM. However, as the concentrations used in this study are much higher, we expected to see the full effect of the inhibitor. But even though RN showed excellent selectivity to TRPV4 over related TRP receptors (TRPV1, TRPV3 and TRPM8) in previous research, we did not observe complete TRPV4 inhibition after RN administration (39). In general, our data show that TRPV4 is a potent modulator of microglial morphology and migration, which is in line with other research (25, 27, 40). The importance of TRPV4 in microglial

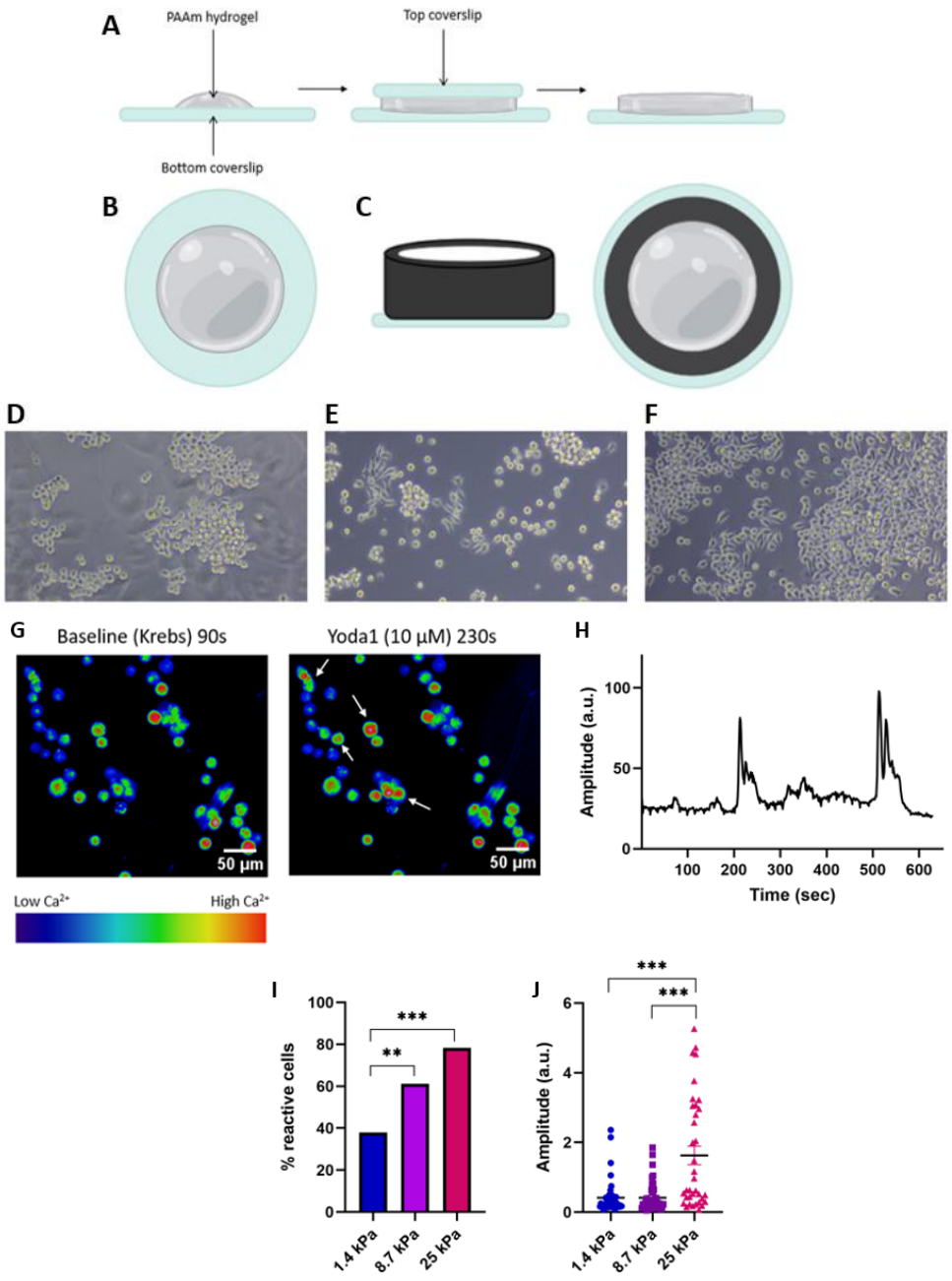

Figure 5: Functional expression of Piezo1 in BV_2 cells in hydroxy-polyacrylamide (PAAm) hydrogels. (**A**) Overview of hydroxy-PAAm hydrogels (side view). (**B**) Top view of finished hydrogel on a glass coverslip. (**C**) Side and top view of custom-made Teflon rings on the hydroxy-PAAm hydrogels to keep the cells centered. (**D-F**) Representative images of BV_2 cells cultured in hydroxy-PAAm hydrogels of 1.4 kPa, 8.7 kPa and 25 kPa, respectively. Images were captured after 5 days in culture. (**G**) Representative images of Fluo-4 labeled BV_2 cells in an 8.7 kPa hydroxy-PAAm hydrogel before (90 sec) and during Piezo1 stimulation (230 sec, examples of reactive cells shown by white arrows) with 10 µM of Yoda1. (**H**) Representative Ca^{2+}-influx trace of BV_2 cells in a 1.4 kPa hydroxy-PAAm hydrogel throughout live-cell Ca^{2+} imaging of Piezo1 stimulation with 10 µM Yoda1, showing 1 peak during Yoda1 stimulation (120-240 sec) and 1 peak during ATP stimulation (480-540 sec). (**I**) Percentage of BV_2 cells in hydroxy-PAAm hydrogels of 1.4 kPa (37.9%), 8.7 kPa (61.11%) and 25 kPa (78.26%) reactive to Piezo1 stimulation with 10 µM of Yoda1. (**J**) Ca^{2+} response of reactive BV_2 cells in 1.4 kPa, 8.7 kPa and 25 kPa hydroxy-PAAm hydrogels represented as the amplitude during administration of 10 µM Yoda1 ($n_{1.4kPa}$= 47, $n_{8.7kPa}$= 44, n_{25kPa}= 36). Data are represented as mean ± SEM and analyzed using (**I, J**) Kruskal-Wallis with Dunn's correction for multiple comparisons. **p<0.01, ***p<0.001.

functions is also evident in the branch motility analysis, which shows that wild type microglia survey a smaller area, with fewer and shorter filopodia after TPRV4 inhibition.

Because Beeken *et al.* found no change in branch motility in *Trpv4*$^{-/-}$ microglia, we believed another mechanosensitive channel compensated for *Trpv4* deficiency. However, we found no upregulation of *Piezo1, Piezo2, Trpm7* and *Trpm2* in *Trpv4*$^{-/-}$ microglia. In contrast to what we expected, we even observed a lower expression level of *Piezo1* and *Trpm7*, though not significant. This could indicate that the differences in morphology and migration in *Trpv4*$^{-/-}$ microglia *in vivo* are also due to a possible downregulation of e.g. Piezo1. However, this requires further research. Due to the high variability in this data, single-cell sequencing might give a clearer view of these channels' expression.

Piezo1 has been implicated in regulating microglial functions during hyperglycemic stress (17). It has also been established that Piezo1 plays a role in mediating cell migration (41). Hence, we further investigated the functional expression of *Piezo1* in microglia by live-cell Ca^{2+} imaging after Piezo1 stimulation with Yoda1. We demonstrated Ca^{2+}-influx in the soma of murine WT microglia following acute Piezo1 activation.

Next, we evaluated the effect of TRPV4 and Piezo1 activation on microglial morphology and migration, using agonists GSK1016790A and Yoda1, respectively. Both GSK101 concentrations and 0.2 µM Yoda1 increased cell circularity in the first half-hour after incubation, though that effect was already lost after 6 h of incubation. The effect of 0.2 µM of Yoda1 opposes other studies reporting that 5 µM of Yoda1 does not alter microglial morphology (42). However, they used higher concentrations (5-20 µM Yoda1) for functional studies. In this study, when looking at the functional expression of Piezo1 (live-cell Ca^{2+} imaging), we incubated microglia and BV_2 cells with Yoda1 ranging from 10 to 50 µM.

Unfortunately, the evaluation of the effect of TRPV4 and Piezo1 activation on microglial migration is still ongoing, and the role of Piezo1 in microglial branch motility still needs to be investigated. Another direction in research that hasn't been pursued yet is the effect of Piezo1 inhibition on microglial functions.

One noticeable element in our results is that both inhibition and activation of TRPV4 seem to decrease morphological complexity. It might be possible that both manipulations indeed lead to the same result, but due to different reasons. After TRPV4 inhibition, the cell gets rounder due to a lack of $[Ca^{2+}]_i$, meaning it cannot remodel the cytoskeleton to form branches. Activation of TRPV4, on the other hand, might lead to the activation of the entire microglia, after which the cell often retracts its branches and takes on an amoeboid-like morphology (5, 25, 27). In contrast to our results, Chubinskiy-Nadezhdin *et al.* found a decrease in cell roundness after administration of 30 µM of Yoda1 to fibroblasts (43).

In the last part of this study, we investigated if and how the mechanical properties of the ECM, more specifically its stiffness, affected cell morphology and migration. For this, we used hydroxy-PAAm hydrogels based on the protocol of Grevesse *et al.* (36). Compared to previous techniques, this new approach does not require expensive chemical compounds or deep UV irradiation, as it uses a commercial acrylamide monomer with hydroxyl groups. Another benefit is that they allow independent tuning of the substrate stiffness. Unfortunately, we were not able to optimize the culture conditions for isolated murine microglia in hydroxy-PAAm hydrogels. BV_2 cells did attach to these hydrogels, and we were able to perform a functional analysis on the Piezo1 expression in these cells in hydrogels of varying stiffness. The stiffer the substrate, the more cells responded and the higher the response was. Isolated murine microglia, however, did not attach to these substrates, even though they did attach to the glass coverslip outside of the gels. This could be due to not having the optimal coating conditions yet for the hydrogels. In this study, we used PDL and collagen-IV to coat the hydrogels. Other options to be tested include laminins or fibronectin. Bollman *et al.* have produced hydroxy-PAAm hydrogels of varying stiffness' and cultured isolated microglia in them (16). However, they use expensive chemical compounds. Another option to optimize the protocol is to place a polydimethylsiloxane (PDMS) microstamp on the hydroxy-PAAm hydrogels to create a specific area on the hydrogel where the cells can attach and grow (36). A second factor that might still need optimization in this process is the density of the cells. Throughout this

study, we have seeded isolated microglia in various densities, ranging from 50 000 – 200 000 cells per well (in a 12-well plate), to see if a higher density might stimulate attachment to the hydrogels. Unfortunately, we observed the same result in different densities.

It is crucial to get a better perception of microglial functions in a healthy condition so that we can determine what goes wrong in neurological diseases and disorders. For example, in spinal cord injuries, the tissue around the lesion gets stiffer due to scar formation (44). And in Alzheimer's disease, stiff amyloid-beta plaques form and tissue stiffness has been shown to be influenced by the disease severity (45, 46). Understanding the influence of the surrounding tissue stiffness on microglial functions thus will help us understand the role of microglia in these pathological conditions.

CONCLUSION

In conclusion, this study further demonstrates the importance of TRPV4 in regulating microglial morphology, migration and branch motility. It also explored the role of Piezo1 in microglia, as this has not been done before. The insights into the working mechanisms of these mechanosensitive channels in healthy microglia may ultimately contribute to the development of therapies for neurological disorders involving microglial dysfunction.

REFERENCES

1. Smolders SM, Kessels S, Vangansewinkel T, Rigo JM, Legendre P, Brône B. Microglia: Brain cells on the move. Prog Neurobiol. 2019;178:101612.
2. Colonna M, Butovsky O. Microglia Function in the Central Nervous System During Health and Neurodegeneration. Annu Rev Immunol. 2017;35:441-68.
3. Sominsky L, De Luca S, Spencer SJ. Microglia: Key players in neurodevelopment and neuronal plasticity. The International Journal of Biochemistry & Cell Biology. 2018;94:56-60.
4. Madry C, Attwell D. Receptors, ion channels, and signaling mechanisms underlying microglial dynamics. J Biol Chem. 2015;290(20):12443-50.
5. Jurga AM, Paleczna M, Kuter KZ. Overview of General and Discriminating Markers of Differential Microglia Phenotypes. Frontiers in Cellular Neuroscience. 2020;14.
6. Dubbelaar ML, Kracht L, Eggen BJL, Boddeke EWGM. The Kaleidoscope of Microglial Phenotypes. Front Immunol. 2018;9:1753-.
7. Lau LW, Cua R, Keough MB, Haylock-Jacobs S, Yong VW. Pathophysiology of the brain extracellular matrix: a new target for remyelination. Nature Reviews Neuroscience. 2013;14(10):722-9.
8. Kim Y, Meade SM, Chen K, Feng H, Rayyan J, Hess-Dunning A, et al. Nano-Architectural Approaches for Improved Intracortical Interface Technologies. Frontiers in Neuroscience. 2018;12.
9. Thomsen MS, Routhe LJ, Moos T. The vascular basement membrane in the healthy and pathological brain. J Cereb Blood Flow Metab. 2017;37(10):3300-17.
10. van 't Spijker HM, Kwok JCF. A Sweet Talk: The Molecular Systems of Perineuronal Nets in Controlling Neuronal Communication. Frontiers in Integrative Neuroscience. 2017;11.
11. Färber K, Kettenmann H. Functional role of calcium signals for microglial function. Glia. 2006;54(7):656-65.
12. Mizoguchi Y, Monji A. Microglial Intracellular Ca(2+) Signaling in Synaptic Development and its Alterations in Neurodevelopmental Disorders. Front Cell Neurosci. 2017;11:69.
13. Hepler PK. The Cytoskeleton and Its Regulation by Calcium and Protons. Plant Physiology. 2016;170(1):3-22.
14. Moshayedi P, Costa Lda F, Christ A, Lacour SP, Fawcett J, Guck J, et al. Mechanosensitivity of astrocytes on optimized polyacrylamide gels analyzed by quantitative morphometry. J Phys Condens Matter. 2010;22(19):194114.
15. Jagielska A, Norman AL, Whyte G, Vliet KJ, Guck J, Franklin RJ. Mechanical environment modulates biological properties of oligodendrocyte progenitor cells. Stem Cells Dev. 2012;21(16):2905-14.
16. Bollmann L, Koser D, Shahapure R, Gautier H, Holzapfel G, Scarcelli G, et al. Microglia mechanics: immune activation alters traction forces and durotaxis. Frontiers in Cellular Neuroscience. 2015;9.
17. Liu H, Bian W, Yang D, Yang M, Luo H. Inhibiting the Piezo1 channel protects microglia from acute hyperglycaemia damage through the JNK1 and mTOR signalling pathways. Life Sci. 2021;264:118667.
18. Li X, Wang J. Mechanical tumor microenvironment and transduction: cytoskeleton mediates cancer cell invasion and metastasis. International Journal of Biological Sciences. 2020;16(12):2014-28.
19. Kim J, Lee J, Jang J, Ye F, Hong SJ, Petrich BG, et al. Topological Adaptation of Transmembrane Domains to the Force-Modulated Lipid Bilayer Is a Basis of Sensing Mechanical Force. Current Biology. 2020;30(9):1614-25.e5.

20. Wacker D, Stevens RC, Roth BL. How Ligands Illuminate GPCR Molecular Pharmacology. Cell. 2017;170(3):414-27.
21. Bassilana F, Nash M, Ludwig M-G. Adhesion G protein-coupled receptors: opportunities for drug discovery. Nature Reviews Drug Discovery. 2019;18(11):869-84.
22. Echeverry S, Rodriguez MJ, Torres YP. Transient Receptor Potential Channels in Microglia: Roles in Physiology and Disease. Neurotoxicity Research. 2016;30(3):467-78.
23. Kanju P, Liedtke W. Pleiotropic function of TRPV4 ion channels in the central nervous system. Exp Physiol. 2016;101(12):1472-6.
24. Michalick L, Kuebler WM. TRPV4—A Missing Link Between Mechanosensation and Immunity. Front Immunol. 2020;11.
25. Redmon SN, Yarishkin O, Lakk M, Jo A, Mustafić E, Tvrdik P, et al. TRPV4 channels mediate the mechanoresponse in retinal microglia. Glia. 2021;69(6):1563-82.
26. Konno M, Shirakawa H, Iida S, Sakimoto S, Matsutani I, Miyake T, et al. Stimulation of transient receptor potential vanilloid 4 channel suppresses abnormal activation of microglia induced by lipopolysaccharide. Glia. 2012;60(5):761-70.
27. Nishimoto R, Derouiche S, Eto K, Deveci A, Kashio M, Kimori Y, et al. Thermosensitive TRPV4 channels mediate temperature-dependent microglia movement. Proceedings of the National Academy of Sciences. 2021;118(17):e2012894118.
28. Coste B, Mathur J, Schmidt M, Earley TJ, Ranade S, Petrus MJ, et al. Piezo1 and Piezo2 are essential components of distinct mechanically activated cation channels. Science. 2010;330(6000):55-60.
29. Press release: The Nobel Prize in Physiology or Medicine 2021 NobelPrize.org: Nobel Prize Outreach AB 2022.; 2021 [Available from: https://www.nobelprize.org/prizes/medicine/2021/press-release/.
30. Faucherre A, Kissa K, Nargeot J, Mangoni ME, Jopling C. Piezo1 plays a role in erythrocyte volume homeostasis. Haematologica. 2014;99(1):70-5.
31. Pathak MM, Nourse JL, Tran T, Hwe J, Arulmoli J, Le DT, et al. Stretch-activated ion channel Piezo1 directs lineage choice in human neural stem cells. Proc Natl Acad Sci U S A. 2014;111(45):16148-53.
32. Wang L, You X, Lotinun S, Zhang L, Wu N, Zou W. Mechanical sensing protein PIEZO1 regulates bone homeostasis via osteoblast-osteoclast crosstalk. Nat Commun. 2020;11(1):282.
33. Kang H, Hong Z, Zhong M, Klomp J, Bayless KJ, Mehta D, et al. Piezo1 mediates angiogenesis through activation of MT1-MMP signaling. Am J Physiol Cell Physiol. 2019;316(1):C92-c103.
34. Bohlen CJ, Bennett FC, Bennett ML. Isolation and Culture of Microglia. Curr Protoc Immunol. 2019;125(1):e70-e.
35. Bohlen CJ, Bennett FC, Tucker AF, Collins HY, Mulinyawe SB, Barres BA. Diverse Requirements for Microglial Survival, Specification, and Function Revealed by Defined-Medium Cultures. Neuron. 2017;94(4):759-73.e8.
36. Grevesse T, Versaevel M, Gabriele S. Preparation of hydroxy-PAAm hydrogels for decoupling the effects of mechanotransduction cues. J Vis Exp. 2014(90):51010.
37. Bachiller S, Jiménez-Ferrer I, Paulus A, Yang Y, Swanberg M, Deierborg T, et al. Microglia in Neurological Diseases: A Road Map to Brain-Disease Dependent-Inflammatory Response. Frontiers in Cellular Neuroscience. 2018;12.
38. Franco-Bocanegra DK, McAuley C, Nicoll JAR, Boche D. Molecular Mechanisms of Microglial Motility: Changes in Ageing and Alzheimer's Disease. Cells. 2019;8(6):639.

39. Wei Z-L, Nguyen MT, O'Mahony DJR, Acevedo A, Zipfel S, Zhang Q, et al. Identification of orally-bioavailable antagonists of the TRPV4 ion-channel. Bioorganic & Medicinal Chemistry Letters. 2015;25(18):4011-5.
40. Wang Z, Zhou L, An D, Xu W, Wu C, Sha S, et al. TRPV4-induced inflammatory response is involved in neuronal death in pilocarpine model of temporal lobe epilepsy in mice. Cell Death & Disease. 2019;10(6):386.
41. Canales Coutiño B, Mayor R. Mechanosensitive ion channels in cell migration. Cells & Development. 2021;166:203683.
42. Konttinen H, Sitnikova V, Ishchenko Y, Shakirzyanova A, Giudice L, Ugidos IF, et al. Microglial amyloid beta clearance is driven by PIEZO1 channels. bioRxiv. 2022:2022.03.18.484831.
43. Chubinskiy-Nadezhdin VI, Vasileva VY, Vassilieva IO, Sudarikova AV, Morachevskaya EA, Negulyaev YA. Agonist-induced Piezo1 activation suppresses migration of transformed fibroblasts. Biochemical and Biophysical Research Communications. 2019;514(1):173-9.
44. O'Shea TM, Burda JE, Sofroniew MV. Cell biology of spinal cord injury and repair. J Clin Invest. 2017;127(9):3259-70.
45. Murphy MC, Jones DT, Jack CR, Glaser KJ, Senjem ML, Manduca A, et al. Regional brain stiffness changes across the Alzheimer's disease spectrum. NeuroImage: Clinical. 2016;10:283-90.
46. Hall CM, Moeendarbary E, Sheridan GK. Mechanobiology of the brain in ageing and Alzheimer's disease. European Journal of Neuroscience. 2021;53(12):3851-78.

Acknowledgments – Bieke Janssen is grateful to be allowed to do an internship in the research group of Prof. dr. Bert Brône. She is thankful for the help of Femke Mussen, a fellow student, and Melanie Mertens with performing experiments and analyzing data. She wants to thank dr. Yeranddy A. Alpizar for the excellent guidance and valuable feedback. She thanks Imo-imomec for the use of their UV/Ozone cleaner. Lastly, dr. Yeranddy A. Alpizar, Melanie Mertens and Femke Mussen are thanked for their pleasant cooperation during this internship.

Author contributions – YAA designed the research and experiments. BJ, FM and MM performed experiments and analyzed data under the supervision of YAA. BB contributed to data interpretation. BJ wrote the paper, and YAA carefully edited the manuscript.

SUPPLEMENTARY INFORMATION

Genotyping – Newborn pups were genotyped for *Cx3cr1*-eGFP on postnatal day 7-12, using PCR. DNA was extracted from toe biopsies with 10x Kapa Express extraction buffer, 1 U/µl Kapa Express extraction enzyme (KAPA Biosystems, USA) and Milli-Q water for 15 min at 75 °C. Next, the DNA samples were diluted in a PCR-solution containing 10 µM of each primer for *Cx3cr1* (**Suppl. table 1**) in Kapa2G Fast genotyping mix (KAPA Biosystems, USA). DNA was then amplified following a specific PCR program (**Suppl. table 2**). The samples were loaded on a 3% agarose gel, made from UltraPure Agarose (Invitrogen, Waltham, MA, USA), TAE 1x GelRed (1/10000, Biotium, Fremont, CA, USA), along with a 200-10 000 bp DNA SmartLadder (Eurogentec, Seraing, Belgium) as a control. Migration was launched at 160 V. Lastly, gels were read using D-Digir (LI-COR Biosciences, Germany)

Suppl. table 1: Cx3Cr1-eGFP Primer sequences

Forward	5' CTC CCC CTG AAC CTG AAA C 3' 5' GTC TTC ACG TTC GGT CTG GT 3'
Reverse	5' CCC AGA CAC TCG TTG TCC TT 3'

Suppl. table 2: *Cx3Cr1*-eGFP PCR program

1	94 °C	2 min	X1
2	94 °C	30 sec	X10
	65 °C	1 min	
	68 °C	1 min	
3	94 °C	30 sec	X28
	60 °C	1 min	
	72 °C	1 min	
4	72 °C	2 min	X1
5	15 °C	For ever	

Quantitative real-time PCR – RNA was isolated from cultured WT and *Trpv4*$^{-/-}$ murine microglia with the RNeasy Mini Kit (Qiagen, Germany) following manufacturer's instructions. The NanoDrop 2000 (ThermoFisher Scientific) was used to assess purity and concentration. cDNA was synthesized through reverse transcription with the qScript cDNA SuperMix (VWR, Radnor, US) and diluted to a final concentration of 5 ng/µl. The cDNA was amplified by real-time PCR on the StepOnePlus Real-Time PCR system (Applied Biosystems, Foster City, US) using the SYBR Green Master Mix (Applied Biosystems), probes for *Piezo1*, *Piezo2*, *Trpm7*, *Trpm2* and *Gapdh* and the following program (**Suppl. table 3**). Expression of these genes was measured and represented using the comparative C_T method (dC_T) with *Gapdh* as a reference gene.

Suppl. table 3: qPCR program

1	95 °C	20 sec	X1
2	95 °C	30 sec	X40
	60 °C	30 sec	
3	95 °C	15 sec	X1
	60 °C	1 min	
	95 °C	15 sec	
5	4 °C	For ever	